Journal of Structural Geology, Vol. 9, No. 1, pp. 71 to 86, 1987
Printed in Great Britain

0191-8141/87 $03.00 + 0.00

Fracture propagation associated with dike emplacement at the Skaergaard intrusion, East Greenland

RALPH D. ROGERS

School of Geology and Geophysics, University of Oklahoma, Norman, OK 73019, U.S.A.

and

DENNIS K. BIRD

Department of Geology, Stanford University, Stanford, CA 94305, U.S.A.

(*Received* 10 *December* 1985; *accepted in revised form* 2 *July* 1986)

Abstract—Extensive magmatic activity, including several episodes of dike emplacement, was associated with early Tertiary continental rifting in Eastern Greenland. Exposures of the Skaergaard intrusion host a large number of these dikes as well as a variety of hydrothermal veins. One vein set has a characteristic outcrop expression and is filled with silica-rich chlorites. Relative timing constraints as well as the distribution and geometric relations of these veins relative to the mafic dikes indicate that at least some of these fractures formed during the emplacement of the dikes that cut the intrusion. Calculations based on elastic theory permit modeling of dike geometries observed in the field and prediction of fracture geometries that could be associated with the inflation of these dikes. Extensional fractures may form in the area ahead of the dike termination for a variety of loading conditions. The predicted width to length ratio for the dike as well as the size of the predicted fracture zone increases with increasing magma pressure within the dike and/or increasing differential between the remote principal stresses. For dike geometries similar to those observed in the field, the predicted fracture zone is roughly elliptical in cross-section and is centered in front of the dike termination. The size of the zone perpendicular to the dike trend varies from less than one meter to several meters. Field observations indicate that dike-parallel fractures are locally offset normal to the dike margin by distances of a few centimeters to a few meters. Our analysis implies that at least some of these fractures initiated and propagated ahead of the dikes as they were emplaced. The cooling of these dikes initiated localized hydrothermal systems that formed the vein minerals currently filling the fractures.

INTRODUCTION

EARLY TERTIARY continental rifting in East Greenland was accompanied by extensive magmatism, including several episodes of dike emplacement (Fig. 1). The Skaergaard intrusion is one of several layered gabbros in this region that host these dikes (Wager & Deer 1939, Nielsen 1978). Because the lithologic characteristics, petrogenetic and structural history of this intrusion are simple and well known, it provides an unusually well constrained data base for studies of dike emplacement. A number of mineralized fracture systems have been identified within the Skaergaard intrusion (Norton *et al.* 1984, Bird *et al.* 1987). One fracture set has a distinct outcrop expression, weathering rust-brown. This fracture set is filled with a characteristic alteration mineralogy and is invariably found near mafic dikes. Relative timing constraints and geometric relations indicate that the fractures hosting these veins may have formed as an integral part of the process of dike emplacement.

A number of workers have suggested that fracturing occurs in the host rocks of sheet intrusions, such as dikes and sills (Roberts 1970, Pollard 1973, Kokelaar 1982, Delaney *et al.* 1986). Savage & Cockerham (1984) have related present day seismicity in the Long Valley Caldera to dike inflation. In cases where this fracturing leads to brecciation of the host rocks the relationship to the sheet intrusion is clear (Kokelaar 1982, Delaney & Pollard 1981). However, in cases where the fractures parallel the sheet intrusion the genetic relationship is less clear because the dike may be following a pre-existing fracture set (Delaney *et al.* 1986).

An extensive literature exists on the applications of elastic theory to problems associated with fracture initiation and propagation. In particular, a number of workers have developed elastic models that can be applied to dikes, building on the classic work of Anderson (1936). Most of these models focus on the dike termination, modelling the dike as a fluid filled crack in an elastic medium (Pollard 1973). Beach (1980) presented a detailed discussion of the criteria for propagation of such a flaw in the static case and Spence & Turcotte (1985) have developed a solution that includes an evaluation of fluid flow within the dike. Weertman (1971) employed dislocation theory to investigate problems of magma transport. Analytical solutions for stress distributions around elliptical magma chambers and predictions of secondary fracturing in the surrounding medium are presented by Robson & Barr (1964), Roberts (1970) and Koide & Bhattacharji (1975). Similar elastic models have been used to investigate the dilation of dike walls (Delaney & Pollard 1981), to evaluate the mechanical

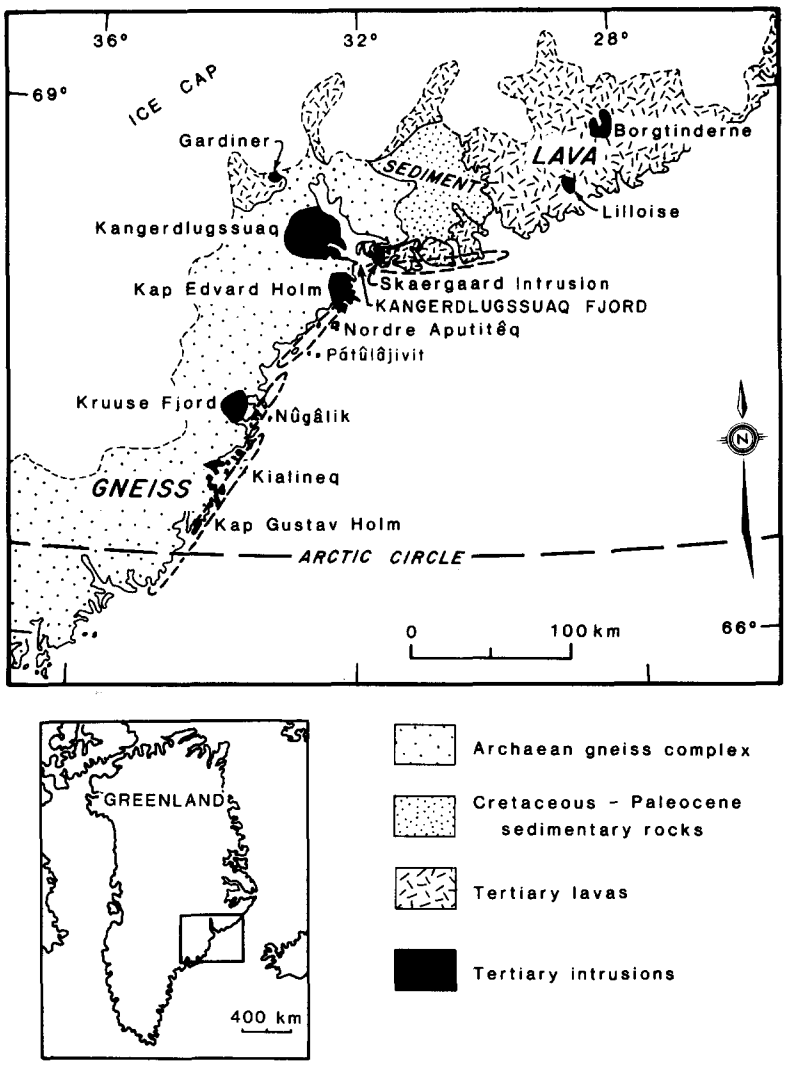

Fig. 1. Generalized geological map of the East Greenland Tertiary igneous province showing the regional distribution of the coast-parallel dike swarms. Modified from Myers (1980), Bridgwater *et al.* (1978), Wager & Brown (1967) and Brooks & Nielsen (1982).

interactions between a dike and a free surface (Pollard & Holzhausen 1979) and the interactions of dikes forming an echelon array (Pollard *et al.* 1982). Elastic models have also been used to estimate stresses and to predict fracture initiation that results from heat transfer away from igneous bodies (Knapp & Norton 1981, Marsh 1982). Heat transfer can also initiate fractures as a result of anomalous pore fluid pressures developed in the host rocks of the igneous bodies (Knapp & Knight 1977, Delaney 1982). Pollard *et al.* (1983) have investigated surface deformation and fracturing in volcanic rift zones that is related to dike emplacement at depth. These studies have provided important information concerning the physical processes associated with the initiation and propagation of dikes and veins in geological environments.

In this communication we build upon these previous studies by using an elastic model to predict zones of potential fracture initiation in the gabbroic host rocks of mafic dikes cutting the Layered Series gabbros of the Skaergaard intrusion. Comparative analysis of the numerical results with chlorite-filled fracture distributions mapped in the field permits evaluation of the relative magnitudes of the remote stresses, magma pressure within the dikes and interstitial pore fluid pressure within the gabbroic host rocks associated with the emplacement of the mafic dikes and initiation of secondary fractures. We also use our two-dimensional elastic model to characterize the cross-sectional area of a zone of potential fracturing associated with the dike terminations and discuss the process of fracture propagation associated with dike emplacement.

FRACTURE SYSTEMS OF THE SKAERGAARD INTRUSION

The Skaergaard magma chamber inflated along the unconformity between Precambrian crystalline basement and overlying Cretaceous sediments and Tertiary basalts (Wager & Deer 1939). This intrusion is oval in outcrop with dimensions of $\cong 8 \times 12$ km (Fig. 2).

The earliest fracturing event within the Skaergaard intrusion was associated with remobilization of residual

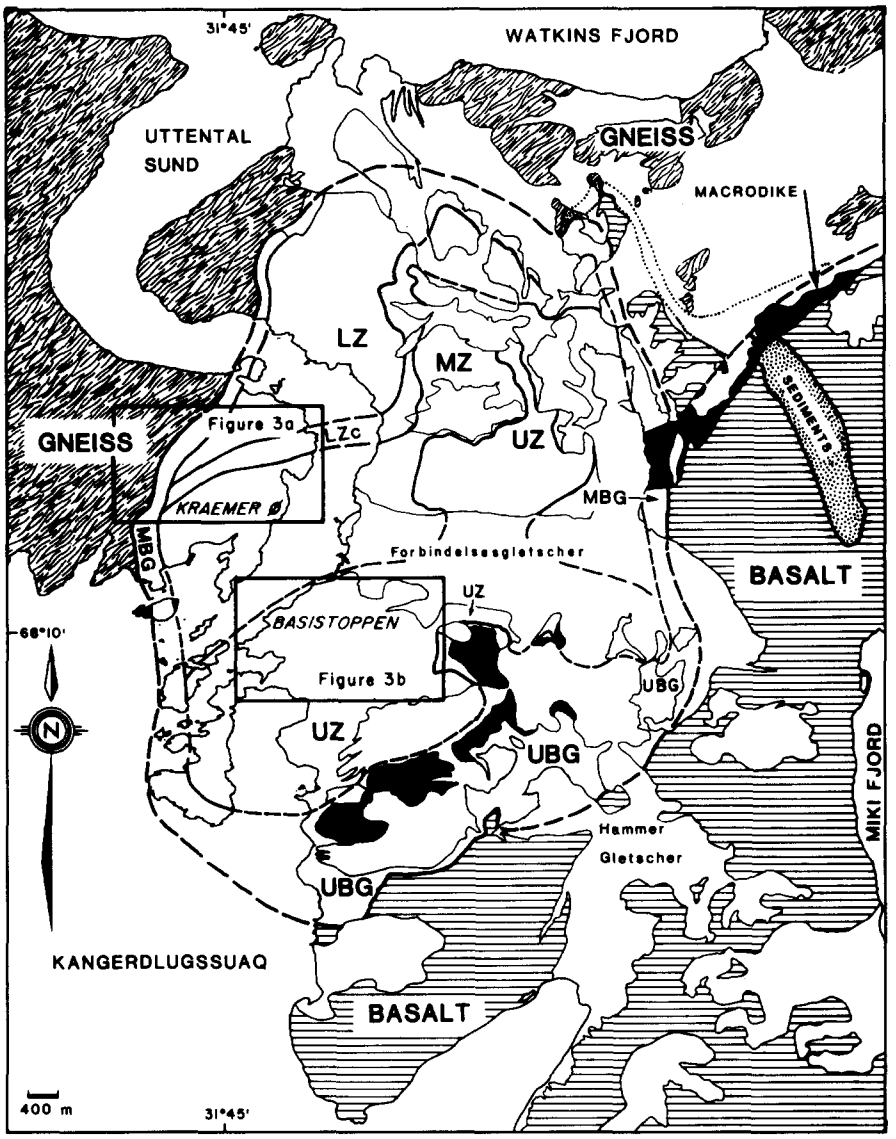

Fig. 2. Generalized geological map of the Skaergaard intrusion. Lithologic units within the intrusion include the Layered Series gabbros that are divided into the Lower Zone (LZ), Middle Zone (MZ) and Upper Zone (UZ). UBG and MBG denote the Upper Border Group and Marginal Border Group respectively. Solid black areas within the intrusion represent the Basistoppen Sheet. Map compiled from Wager & Brown (1967) and A. R. McBirney (Pers. Comm. 1984).

magma that formed gabbro pegmatites in fractures that are typically concordant with the igneous layering (McBirney & Noyes 1979). The second event involved the formation of near vertical fracture systems that acted as fluid flow channels for hydrothermal solutions (Norton *et al.* 1984). These fractures weather black in outcrop. They are up to several millimeters wide, are continuous for tens of meters and occur with a frequency that commonly exceeds one fracture per meter throughout the Layered Series gabbros (Bird *et al.* 1987). Based on the compositional relations of hydrothermal clinopyroxene, hornblende and biotite in these veins, it is evident that they formed at temperatures greater than 500–750°C (Manning & Bird 1986). These high temperature veins are cross-cut by acid granophyres that do not have chilled margins with the gabbros and a closely related set of drusy amphibole mineralized veins. Mineralized fractures formed during the final stages of the subsolidus cooling history of the Layered Series gabbros contain coexisting actinolite and hornblende with no hydrothermal clinopyroxenes. Late stage epidote-bearing veins are primarily restricted to the upper portions of the intrusion. Mafic dikes and closely related rust-colored chlorite mineralized veins cross-cut all of the fracture systems mentioned above. The youngest fracturing event was associated with calcite and zeolite mineralized fault zones that crosscut the dikes (Bird *et al.* 1985).

Mafic dikes

The Skaergaard intrusion is cut by several generations of mafic dikes (Nielsen 1978) that form a complex grid pattern of fractures that are continuous for distances of less than 1 m to greater than 1 km (Fig. 3). Fine grained chill zones at the dike margins and terminations indicate that these dikes were intruded after the cooling of the Skaergaard intrusion.

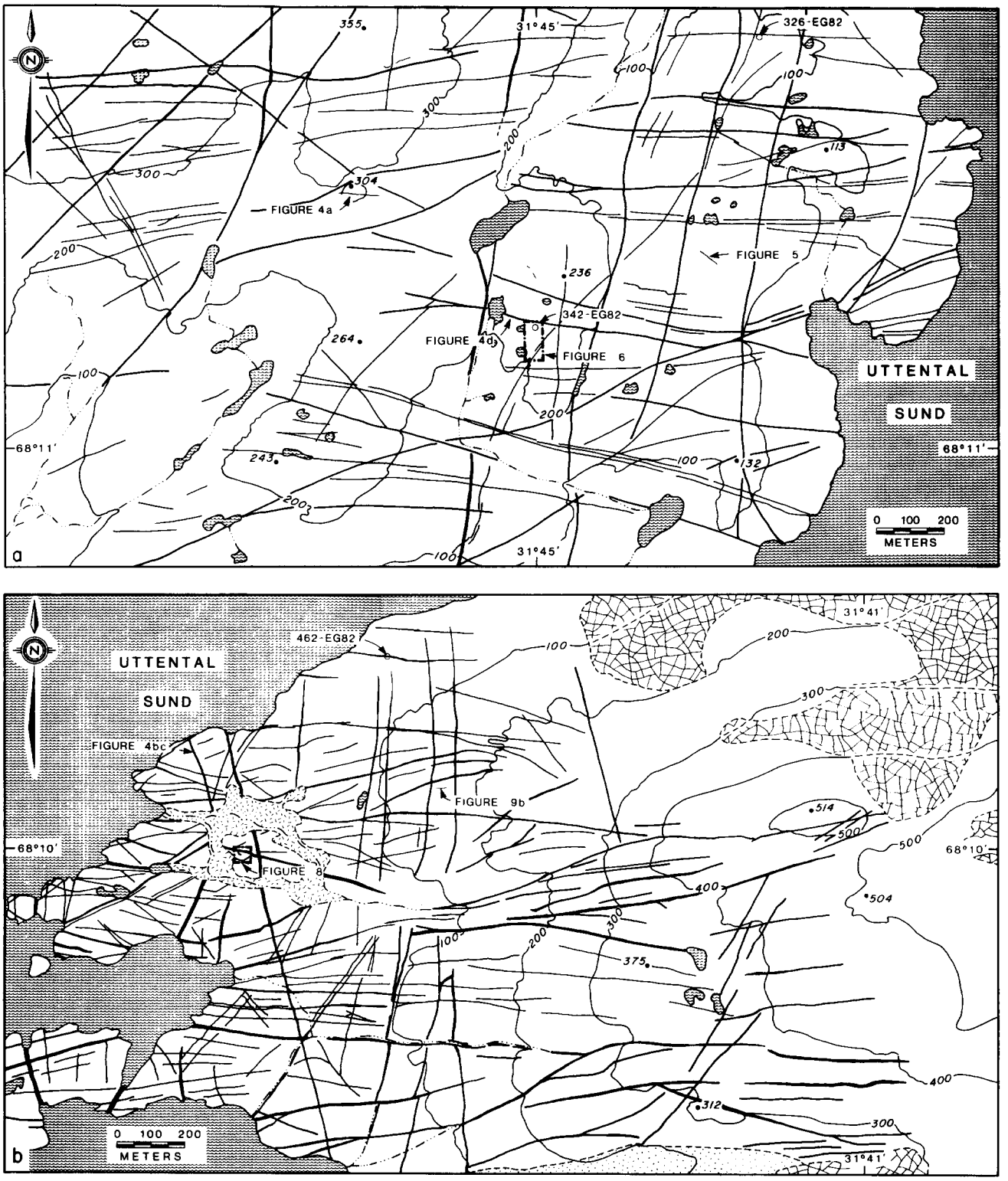

Fig. 3. Air photograph interpretation of dikes cutting the Skaergaard intrusion. Host rocks include the Layered Series gabbros, Marginal Border Group and Precambrian quartzo-feldspathic gneisses. The dominant trend of the dikes is approximately E–W. N–S and NE–SW trends are also present but much less abundant. (a) A portion of Kramer's island. Samples 326-EG82 and 342-EG82 are from chlorite filled veins cutting the Lower Zone and Middle Zone gabbros respectively. (b) West slope of Basistoppen. Sample 462-EG82 is from a chlorite filled vein cutting the Upper Zone *a* gabbros. Locations of the maps are shown on Fig. 2.

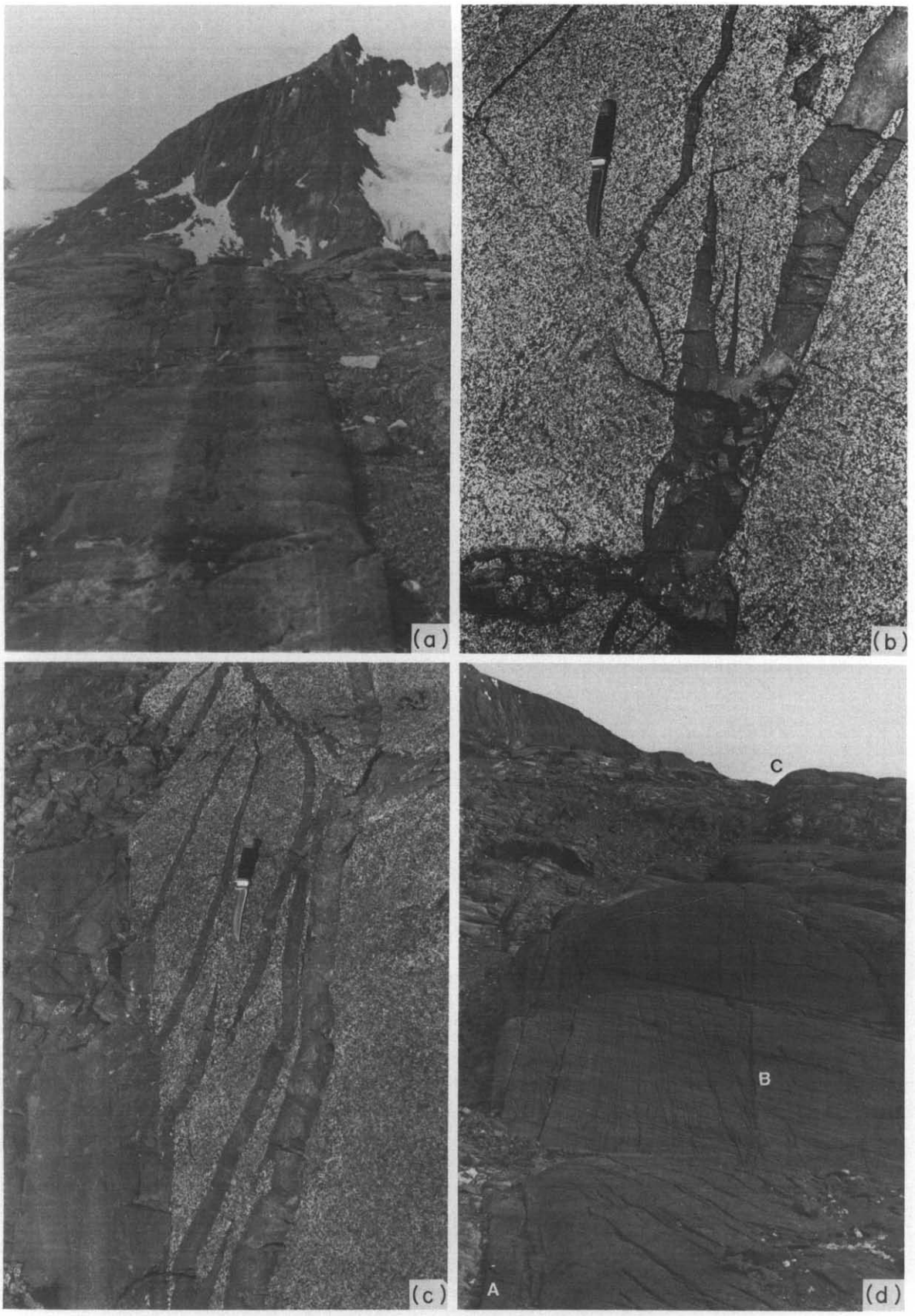

Fig. 4. Mafic dike margins. (a) Dike outcropping on Kramer's island (Fig. 3a). Color banding suggests compositional layering. Contacts between the dikes and the Layered Series gabbros are generally planar. (b) Dike outcropping in Upper Zone *a* gabbros (Fig. 3b). Note spikes of dike material invading country rocks. Fragments of country rock are being engulfed in the upper right-hand corner and lower central parts of the photo. Fine-grained chilled margin material is seen on the photograph as a dark gray zone along the dike margins and surrounding country rock fragments. (c) Dike outcropping in Upper Zone *a* gabbros (Fig. 3b). Spikes of dike material can be seen invading the country rock. These spikes have a tendency to curve into parallelism with the main dike. (d) Fracturing marginal to a mafic dike outcropping on Kramer's island (Fig. 3a). Fractures in the foreground are exposed on a horizontal surface, the dike margin is located at point A. Fractures in the middle ground are exposed on a vertical surface ≅10 m high (point B). Fracture trends are subparallel to the trend of the associated dike. Point C shows the location of Fig. 6.

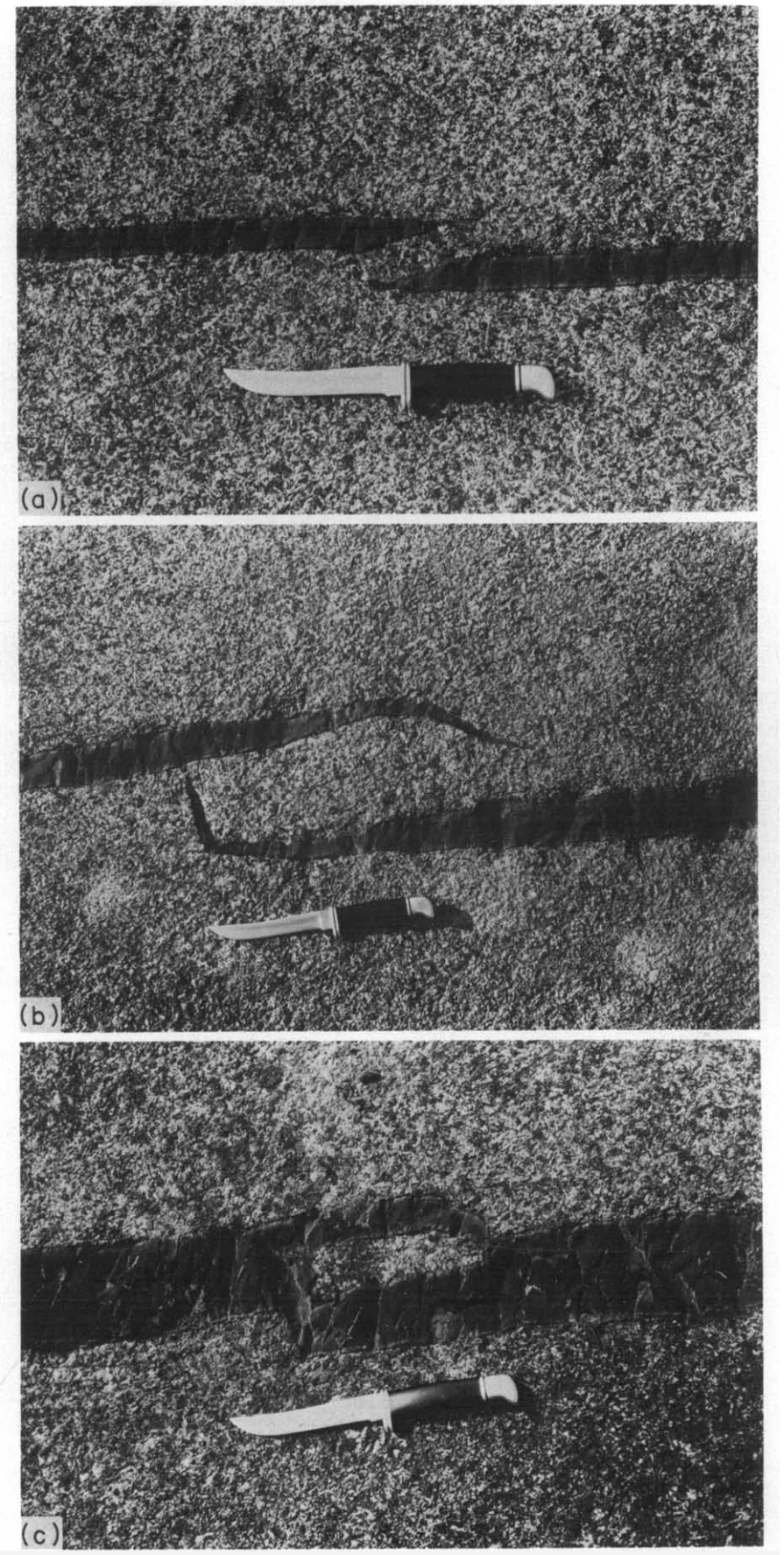

Fig. 5. Mechanical interaction of mafic dike segments outcropping on Kramer's island (Fig. 3a). The terminations of the dike segments exhibit geometries indicative of elastic deformation of the wallrocks during the emplacement of the segments. (a) The terminations are sharpened and asymmetric due to the mechanical interaction. (b) The terminations have followed curved propagation paths probably resulting from their mechanical interaction. (c) Country rock fragment enclosed by mafic dike material. This is interpreted as a case where two offset dike terminations have coalesced trapping the country rock fragment. (a), (b) and (c) occur together over a distance of less than 5 m in one outcrop.

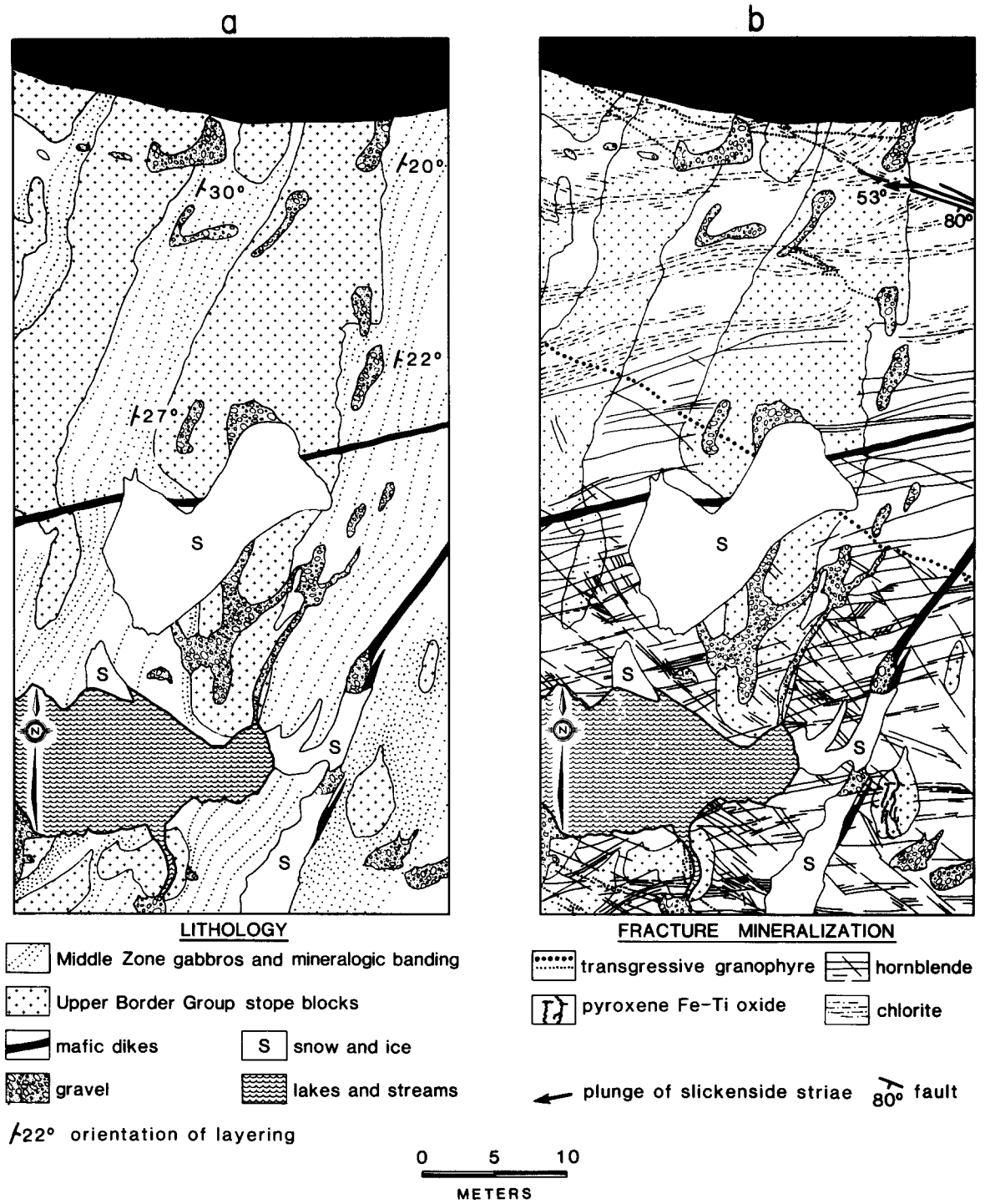

Fig. 6. (a) Geology of a portion of the Middle Zone of the Layered Series gabbros on Kramer's island (Fig. 3a). Blocks of Upper Border Group that have fallen into the magma chamber are common in this area. Bounding the map area to the north is an E–W trending mafic dike approximately 10 m wide. (b) Fracture systems hosting hydrothermal veins. Chlorite mineralized veins are clearly restricted to the area near the dike margin and are subparallel to the trend of the dike. Chlorite vein abundances are shown schematically because the scale of the map would not permit all of them to be displayed.

The dominant regional trend of mafic dikes in the Skaergaard intrusion is N70°E to E–W, approximately parallel to the coast-parallel dike swarms to the S and E of the intrusion shown on Fig. 1 (Wager & Deer 1938, Myers 1980, Larsen 1978). N–S and NE–SW trends are also present in significant, though volumetrically smaller, amounts. The petrology and geochemistry of these dikes have been investigated by Vincent (1953), Brooks & Platt (1975) and Nielsen (1978). The earliest dikes are olivine tholeiites. Later dikes include E–W trending alkaline basalts and lamprophyre dikes with variable chemical characteristics. The youngest dikes are transitional basalts that trend E–W and increase in abundance toward the coastline south of the Skaergaard intrusion. Dike thicknesses vary from a few millimeters to approximately 10 m.

The margins of the dikes are generally simple planar contacts that can be traced for tens to hundreds of meters

(Fig. 4a). The most common deviations from this simple geometry are step-like offsets (Kaitaro 1952) and bayonet-like horns into the wallrocks of the dikes (Fig. 4b). Locally blocks of wallrock have been detached from the walls and engulfed by magma (Fig. 4c).

Microscopically the dike margins are sharp planar contacts lacking evidence of grain-size reduction or replacement of the host gabbros. Geometric relations observed in thin section are similar to larger-scale structures seen in outcrop. Horns of dike material project into the wallrocks for distances comparable to the grain size of the gabbros. Locally fragments of wallrock are surrounded by the dike material. Microfractures filled with chlorite are present near some of the dike margins.

In the field many dikes can be traced to the tip of the fracture, where fine grained chilled magma fills the tip. Where terminations are observed the associated dikes are generally less than about 10 cm thick and consequently the minimum radius of curvature for these terminations is small, usually a few millimeters. Many terminations are essentially triangular in cross-section and taper down to a point. Where dike terminations overlap (Fig. 5) the mechanical interactions between them result in more complicated geometries and may lead to out of plane propagation of the dikes and entrainment of blocks of the host gabbros, similar to features described by Nicholson & Pollard (1985).

At a few localities, fractures hosting mafic dike intrusions continue beyond the terminus of the dike itself. In these cases it is not always possible to tell whether the dike is filling a pre-existing fracture or if the fracture is propagating ahead of the dike as it is emplaced (Currie & Ferguson 1970, Delaney *et al.* 1986). It is apparent in some exposures that mafic dikes intrude along pre-existing hornblende mineralized veins in the Upper Zone gabbros of the Layered Series. Here the hornblende veins are bordered by black <3 cm wide metasomatic reaction zones consisting of chlorite and actinolite that are not present at most dike terminations.

Chlorite veins

In general, there are two major categories of veins in the Layered Series gabbros based on their geometric relations, weathering characteristics and the alteration minerals that fill them. The older vein type usually weathers black and is characterized by hornblende mineralization together with several characteristic types of assemblages that may include pyroxene, biotite, chlorite, actinolite, talc, epidote, prehnite or albite. These veins are associated with the subsolidus cooling history of the Skaergaard intrusion (Norton *et al.* 1984, Bird *et al.* 1987). The younger vein type is characterized by silica-rich chlorites with minor amounts of actinolite and quartz. The chlorite veins are younger, based on cross-cutting relationships observed in the field, and are only found in the vicinity of mafic dikes. They are easily identified in the field by their rust-brown coloration on weathered surfaces.

The map shown in Fig. 6 illustrates the spatial relations

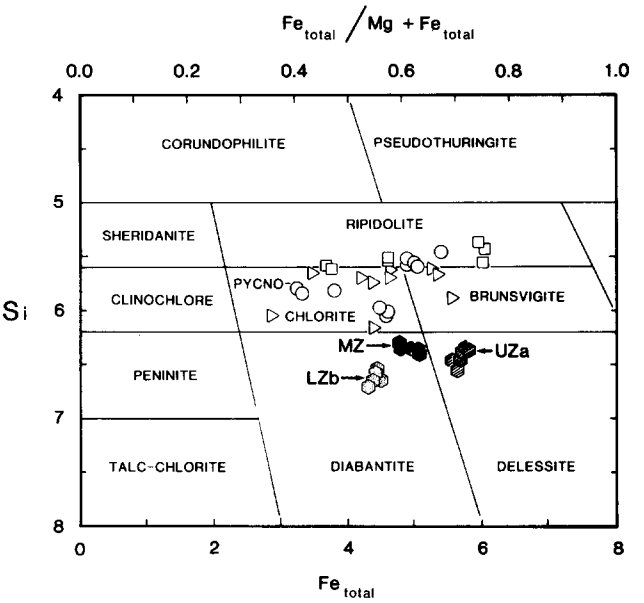

Fig. 7. Compositions of vein chlorites from the Layered Series gabbros. Silica-rich chlorites represented by the hexagons are from chlorite veins associated with mafic dikes. Samples 462-EG82, 342-EG82 and 326-EG82 are represented by the symbols UZa, MZ and LZ, respectively, which represent the stratigraphic zones within the Layered Series gabbros (Fig. 2). Samples are located in Fig. 3. Open symbols denote chlorite compositions in veins formed before the mafic dikes were emplaced. The shape of the open symbols denotes the mineral assemblage coexisting with the chlorite in the vein. Circles represent high temperature clinopyroxene–hornblende–biotite veins, triangles actinolitic hornblende–talc–biotite veins and squares albite–epidote–hornblende veins. Mineralogic data are from Bird *et al.* (1987). Chlorite composition diagram and nomenclature are from Deer *et al.* (1962).

of these two vein types. The chlorite veins (dot-dash lines) are restricted to the area marginal to the mafic dike at the top of the map and are subparallel to the dike margin (Fig. 4d). The hornblende veins (solid lines) are found in the southern part of the map area where they exhibit a variety of orientations. The rust-colored veins are generally less than 1 mm wide and are filled with microcrystalline chlorites and trace amounts of quartz. In some wider veins (0.5–1.5 mm wide) the fluids in the fractures reacted with cumulate pyroxenes to form light-green actinolite in the portions of the fracture that breaks the pyroxene.

The chemistry of chlorites in the rust-colored veins is unique relative to all other vein chlorites found in the Layered Series gabbros. Compositions of chlorites from mafic dike-related veins in Lower Zone *b* (326-EG82), Middle Zone (342-EG82) and Upper Zone *a* (426-EG82) gabbros are given in Fig. 7. The chlorites in veins associated with mafic dikes are silica-rich relative to the more aluminous chlorites found in older types of mineralized fractures in the Layered Series gabbros (Bird *et al.* 1987). It can also be seen in the figure that concentrations of total octahedral iron increase with increasing stratigraphic height in the Skaergaard Layered Series. This possibly reflects the effect of changes in the bulk rock composition, as represented by the Skaergaard fractionation trend, on the compositions of chlorites formed by reactions of aqueous solutions with the wall rock gabbros.

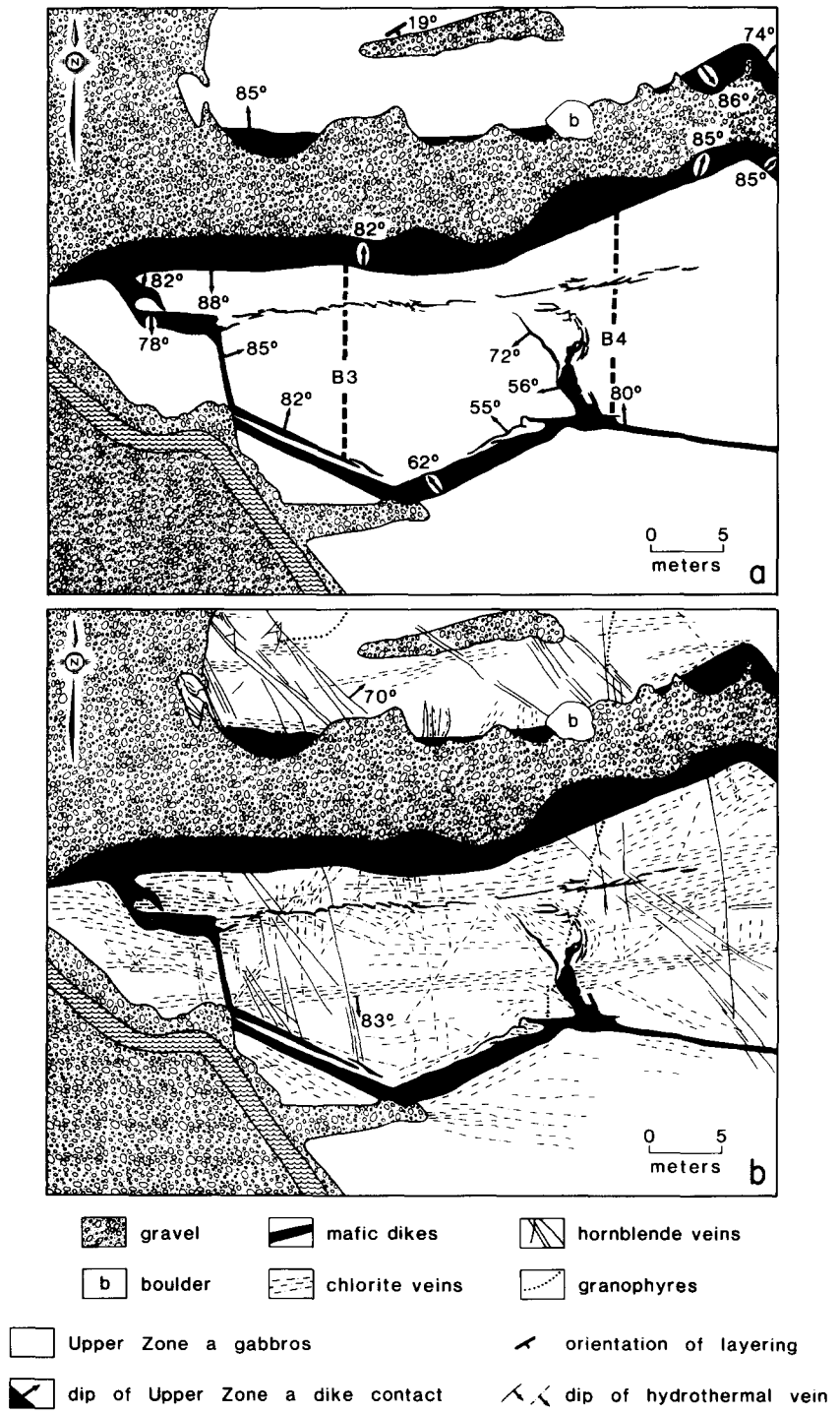

Fig. 8. (a) Mafic dike geometries in a portion of Upper Zone *a* of the layered series (Fig. 3b). All dikes are inferred to connect at depth so that the block in the lower central part of the map is being engulfed by the mafic magma of a large E–W trending dike. Dashed lines marked B3 and B4 locate fracture abundance traverses illustrated on Fig. 10. (b) Fracture systems hosting hydrothermal veins. Hornblende veins and chlorite veins are both present but their geometric relations are very different. The chlorite veins are systematically related to the dike geometries while the hornblende veins show no obvious relationship to the dike geometries.

The abundance of chlorite veins is variable, but tends to increase near dike margins (Fig. 8). These veins are always spatially associated with dikes, but not all dikes have associated chlorite veins. In some cases the chlorite veins are restricted to irregularities along dike margins (Fig. 9b). Fracture abundances measured along traverses perpendicular to dike margins in the Upper Zone *a* gabbros are given on Fig. 10. The number of fractures in a 1 m interval is shown on the histogram as a function of distance from the dike margin. Traverses B3 and B4 were made on the mapped area shown in Fig. 8; they begin and end at dike margins and a small dike segment is present at the point marked by the arrow. Traverse T11 involved only one dike; beyond the 14 m mark on the traverse shown in Fig. 10 no chlorite veins were found. Fracture abundances increase to 5–10 m^{-1}

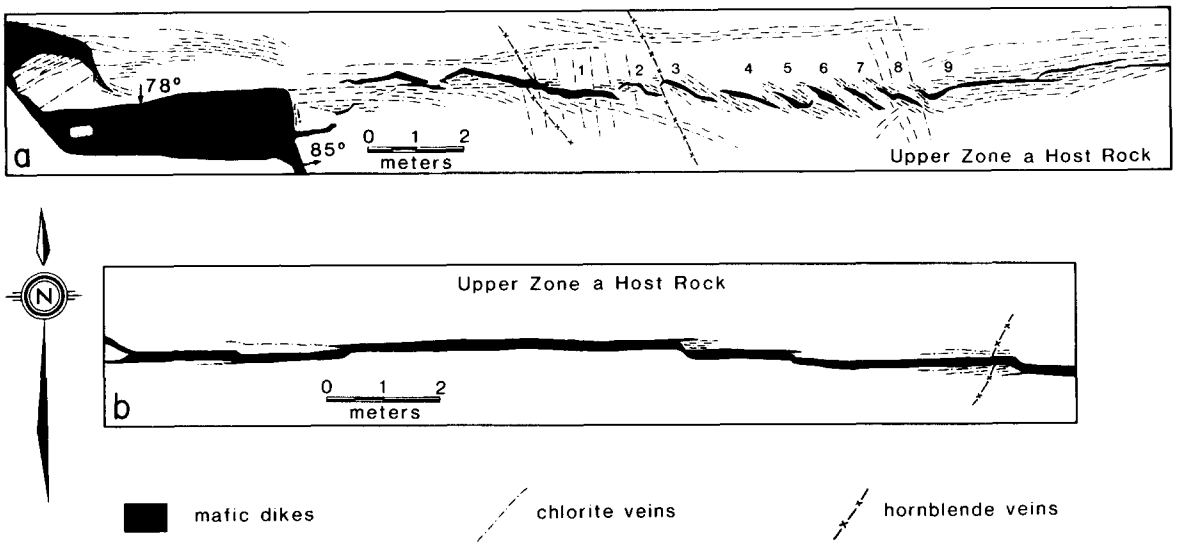

Fig. 9. (a) Echelon array of mafic dike segments from Fig. 8. Map illustrates the details of the dike and fracture geometries. Chlorite veins within the echelon array have different orientations from those outside the array. The chlorite veins commonly extend beyond the terminations of the dike segments and are subparallel to the segments. Fracture abundances are represented schematically. (b) Mafic dike outcropping on the west slope of Basistoppen (Fig. 3b). Step offsets of the dike margin are unusually well displayed. Both right and left stepping offsets are present. Chlorite veins are concentrated near these irregularities along the dike margin.

in the vicinity of these dike margins. These measurements represent the maximum abundances observed. In many outcrops one to five chlorite veins are found, commonly within a few centimeters of the dike margin. Some dikes have no associated chlorite veins.

Evidence for fracturing during dike emplacement

Field relations provide important constraints on the relative ages of fracturing and dike emplacement. Some of the chlorite veins shown in Figs. 8(b) and 9(a) are cross-cut by mafic dikes. Consequently, the fractures hosting these veins cannot be younger than the dikes, but may be contemporaneous. We have not observed any field evidence for dikes intruding along pre-existing chlorite veins. Chlorite veins are younger than the hornblende veins.

In most outcrops chlorite veins are subparallel to mafic dike margins. In a few instances veins perpendicular to the dike margins have been observed (Fig. 8b). The dike-parallel chlorite veins commonly mimic geometric variations in the dikes themselves. An example of this is given in the central portion of Fig. 8, which is a block of the Upper Zone *a* gabbro that is surrounded by mafic dikes. This block is extensively fractured and intruded by a number of small dike segments. The smaller dike segments form an E–W trending echelon array in the NE portion of the block that is shown in detail in Fig. 9(a). In addition, a strongly curved set of dike segments is present in the east central part of the block. Chlorite veins are found subparallel to most of these dike segments and they closely follow the dike geometries. Within the echelon array (Fig. 9a) most chlorite veins are subparallel to the nearest dike segment and where the dike segments are most strongly curved (Fig. 8b) the chlorite veins exhibit a similar curvature. Figure 9(b) shows chlorite veins associated with step offsets of another dike cutting the Upper Zone *a* gabbros. These geometric relations provide strong support for the conclusion that the fractures hosting the chlorite veins formed during dike emplacement.

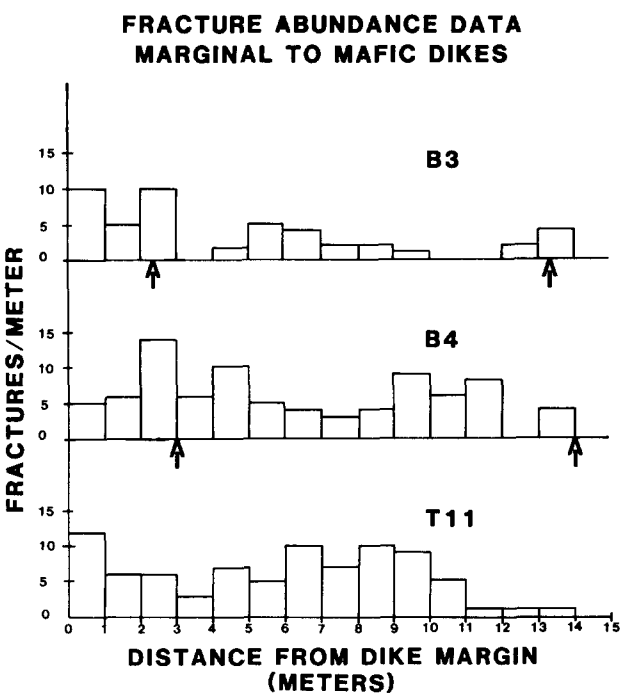

Fig. 10. Fracture abundance measured in traverses perpendicular to the margins of mafic dikes, measured at 1 m intervals and plotted within that interval on the histogram. Each traverse begins at a dike margin. The arrows beneath traverses B3 and B4 indicate the locations of additional dike margins encountered during the traverse. The locations of traverses B3 and B4 are shown on Fig. 8(a).

PREDICTION OF FRACTURE INITIATION

Processes responsible for the formation of the chlorite-filled fractures can be evaluated by numerical models based on the theory of elasticity and linear elastic fracture mechanics (Sneddon & Lowengrub 1969, Broek 1974, Lawn & Wilshaw 1975). As the dikes were emplaced they, no doubt, propagated both vertically and horizontally. However, most of our field data are restricted to fracture geometries observed in a horizontal plane. Consequently, we present a two-dimensional model to evaluate stress distributions in a horizontal plane. This model allows critical analysis of the physical parameters that control fracture initiation in the wallrocks of dikes as well as final dike geometries as observed in outcrop. Emphasis is placed on evaluation of the interactions of remote stresses, magma pressure within the dike and interstitial fluid pressure within the gabbros. In this study we address the following questions: (1) under what conditions is fracture initiation predicted in the vicinity of dike terminations, and (2) what would be the orientation of these predicted fractures?

Stress distributions in the gabbro

Stress distributions in the vicinity of mafic dike terminations are approximated by the boundary element method developed by Pollard (1977), Pollard & Holzhausen (1979) and Segall & Pollard (1980). The method treats the dike as a pressurized crack or set of cracks in a homogeneous elastic medium. The crack wall is divided into a number of segments and the displacement of each segment is calculated as well as the stresses and displacements in the surrounding elastic medium. Consequently, the method permits quantitative analysis of the criteria for fracture initiation in the Layered Series gabbros of the Skaergaard intrusion during the emplacement of the mafic dikes as well as the final equilibrium shape of the dikes.

In the immediate vicinity of a dike termination a zone of tensile stresses is developed (Roberts 1970, Pollard 1973). The size of this zone depends on the difference between the magma pressure in the dike and the magnitude of the remote stress field. As the remote compressive stresses are increased, the size of the tensile stress zone decreases for a given magma pressure. In this study we characterize the size of this tensile stress zone for several limiting loading conditions associated with dike emplacement in the Layered Series gabbros. The presence of alteration minerals along grain boundaries suggests that interstitial fluids were present in the gabbroic host rocks of the dikes. The consequence of interstitial pore fluid pressure is explicitly accounted for in the calculations presented below by use of the concept of "effective stress" (Handin *et al.* 1963, Brace & Martin 1968).

Estimation of model parameters

Stratigraphic reconstructions of the basalts and sediments near the Skaergaard intrusion (Soper *et al.* 1976, Brooks & Nielsen 1982) indicate that the Middle and Upper Zone gabbros studied in this paper were probably emplaced at depths between 5 and 7 km. Nielsen (1978) concluded that most of the dikes considered in this study are only slightly younger than the Skaergaard intrusion itself suggesting similar depths of intrusion for the dikes. Using the minimum thickness of 5 km and a lithostatic gradient of 0.025 MPa m^{-1} requires a confining pressure of $\cong$125 MPa. Similarly, a hydrostatic gradient of 0.01 MPa m^{-1} requires a minimum interstitial fluid pressure of 50 MPa for water filling pores within the gabbro.

The region was undergoing extension and rifting at the time of emplacement of the Skaergaard intrusion and the dikes investigated in this report (Wager & Deer 1938, Brooks & Nielsen 1982). Consequently the least horizontal principal stress would be lower than the lithostatic load during the Early Tertiary magmatic activity. Studies of stress drop associated with earthquakes (Wyss 1970) suggest that the lithosphere is incapable of maintaining a differential stress of more than a few tens of MPa. Consideration of the frictional strength of faulted rock led Zoback (1983) to conclude that differential stress may increase at approximately 10 MPa km^{-1} in extensional environments. As a first approximation the magnitude of the differential stress is varied from 25 to 50 MPa.

Magma pressure can be estimated from dike geometries measured in the field (Pollard 1973). If the dike exhibits an elliptical cross-section perpendicular to the flow direction then the thickness of the dike is controlled by the magma pressure minus the least remote stress divided by the shear modulus of the host rock (Pollard & Muller 1976). Field measurements of dike geometries will constrain this ratio only, but not the absolute magnitudes of magma pressure or remote stress. We have chosen a value of 600 MPa for the shear modulus of the Skaergaard gabbros. This is lower than the values reported for similar rocks by Simmons & Brace (1965) or Birch (1966) because laboratory studies (Heard & Page 1982, Page & Heard 1981) indicate that the shear modulus is lowered by high temperatures. Increasing or decreasing the value of the shear modulus would require similar changes in the values of magma pressure or remote stress in the calculations reported below. The consequences of assuming different values of magma pressure and remote stress will be investigated but the value of the shear modulus will be held constant.

Fracture initiation and orientation

The consequences of adopting physical parameters described above are summarized in Fig. 11 for elastic models of a magma-filled crack 30 m long. This length was chosen because it represents the longest single dike segment mapped in the field. Longer dikes are present (Fig. 3), but we have no data on the cross-sectional geometry of these dikes. Shorter dike segments are also present and we consider these in more detail in the next section.

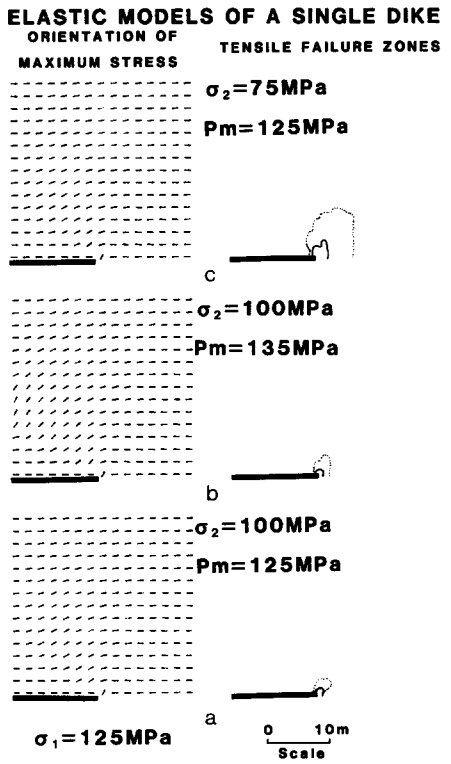

Fig. 11. Results of calculations of stress distributions in an elastic medium surrounding a single dike: (a), (b) and (c) represent different loading conditions. Short dashes on the left half of each figure show the orientation of the maximum compressive stress at selected points in the elastic medium. The right half of each figure shows tensile failure zones associated with the dike terminations. The thin solid lines enclose the tensile failure zone for dry host rocks and the thin dotted line the tensile failure zone for fluid saturated host rocks. The thick solid bar on the figures schematically represents the location of one-half of the dike. In all cases the maximum remote compressive stress is 125 MPa oriented parallel to the dike segment. Loading conditions for the individual cases are: (a) least remote stress is 100 MPa and magma pressure is 125 MPa; (b) least remote stress is 100 MPa and magma pressure is 135 MPa; (c) least remote stress is 75 MPa and magma pressure is 125 MPa.

The orientation of the maximum principal compressive stress at selected points is shown in Fig. 11 for different loading conditions and represents the predicted orientation of extensional fractures at each location. The area where the least principal stress is tensile is also shown. Tensile strength is a notoriously hard parameter to measure; consequently for our calculations we have assumed that the host rocks have zero tensile strength, resulting in the largest possible tensile fracture zone. Our conclusions are not significantly affected unless the tensile strength of the host rocks exceeded 10 MPa. Diagrams in Fig. 11 illustrate the size of the predicted fracture zone for a two-dimensional horizontal section that can be compared to our field maps. Two conditions are shown: the thin solid line outlines the cross-sectional area of the tensile failure zone for a dry host rock and the thin dotted line shows the area where the least effective stress is tensile for an interstitial fluid pressure of 50 MPa.

Dike thicknesses predicted by our model are similar to those observed in the field. For the 30 m long dike in our model thicknesses vary from 0.93 (Fig. 11a) to 1.3 (Fig. 11b) to 1.8 m (Fig. 11c). Some dike outcrops exhibit smaller thickness to length ratios but those predicted by our model include the average values.

The emplacement of the 30 m dike in the model results in distortion of the stress field both ahead of the dike termination and along the dike margin. The greatest distortion in the orientation of the stress field occurs at the dike tip and along the dike margin offset by 5–20 m. In this area the maximum principal stress orientation exhibits great variations from point to point, but ahead of the dike termination the maximum principal stress is everywhere approximately parallel to the dike trend.

The tensile failure zone on Fig. 11 shows the area where at least one of the principal stresses is tensile. For all loading conditions investigated the tensile failure zone increases in size substantially if an interstitial fluid is present in the host rocks of the dikes (compare dotted and solid lines on the right half of Fig. 11). Note that the zone extends further in the direction perpendicular to the dike trend than in the direction parallel to the dike trend and has a roughly elliptical shape in this cross-sectional view.

The calculations summarized on Fig. 11 yield predictions that can be compared to fracture distributions measured in the field. Fractures are predicted in an area ahead of the dike and offset from the trend of the dike. The predicted orientation of fractures in part of this area is parallel to the trend of the dike margin. The size of this predicted failure zone increases substantially if a fluid is present in pores of the host rocks. For the same loading conditions, lengthening the dike would increase the size of the predicted failure zone. Conversely, longer dikes would develop failure zones similar to those shown on Fig. 11 for smaller values of magma pressure and/or smaller differences in the remote compressive stresses.

ANALYSIS OF FRACTURE PROPAGATION

Evidence for fracturing during dike emplacement is well displayed in the maps presented in Figs. 8 and 9. Most of the fractures in Fig. 9(a) are parallel to nearby dike margins. These fractures extend along the dike margins and are not restricted to the area ahead of the dike terminations as suggested by Fig. 11. In order to better understand the possible origins of chlorite vein distributions we have developed models to simulate the emplacement of the dikes in Fig. 9(a). Physical parameters for the dike array models presented below are the same as the single dike model presented in Fig. 11(c), with the least principal remote stress oriented perpendicular to the general trend of the dike segments.

Predictions from the elastic model

The boundary element method allows us to evaluate the effect of mechanical interaction of dike segments on individual dike profiles. Figure 12(a) shows the predicted equilibrium shapes for the dike segments mapped in Fig. 9(a). Deviations of predicted shapes from per-

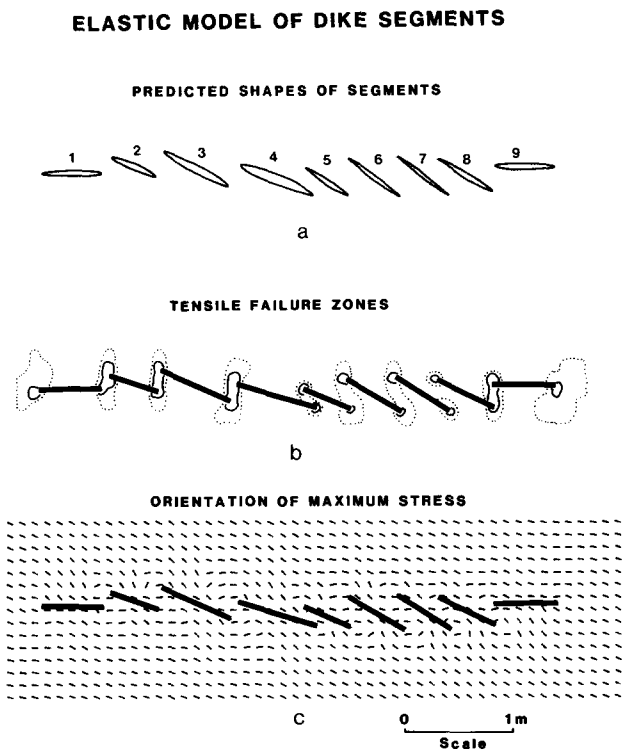

Fig. 12. Elastic model of the dike array shown in Fig. 9(a). Loading conditions for the model are maximum remote compressive stress 125 MPa, least remote stress 100 MPa oriented perpendicular to the trend of the dike segments, and magma pressure within the dike segments 125 MPa. (a) Predicted equilibrium shape of the dike segments. (b) Tensile failure zones. Thin solid lines enclose the areas where the least principal stress is tensile for dry host rocks. Thin dotted lines enclose areas where the least principal effective stress is tensile for interstitial fluids at 50 MPa. Thick solid bars show the locations of the dike segments. (c) Orientation of the maximum principal stress at selected locations in the host rock of the dike segments. Thick solid bars represent the locations of the dike segments.

fectly elliptical cross-sections result from mechanical interactions between the dike segments. Similar deviations from purely elliptical cross-sections can be seen in Fig. 9(a).

The distortion of the stress field caused by the dike array clearly reflects the mechanical interaction of the dike segments. Predicted tensile failure zones in the model (Fig. 12b) are localized near the dike terminations for dry conditions and extend up to 0.25 m into the host rocks if an interstitial fluid is present. In most cases these tensile failure zones are continuous between overlapping dike terminations. Dike emplacement changes the orientation of principal stresses (Fig. 12c) for distances greater than 0.5 m from the dike segments. In general the orientation of the maximum principal stress is parallel to the dike segment along its midsection but is deflected outward near the dike termination. Beyond the termination the maximum principal stress curves back across the dike trend.

Calculations similar to ours have been used by previous workers to estimate fracture toughness, a rock property that is a measure of resistance to fracture propagation (Paris & Sih 1965, Broek 1974, Lawn & Wilshaw 1975). A hydraulic fracture propagates until the mode-I stress intensity factor at its tip falls to a value

Table 1. Mode-I stress intensity factors for dike segments on Fig. 12 (MPa · $m^{1/2}$)

Segment No.	Left termination	Right termination
1	39.9	54.2
2	60.7	59.1
3	63.0	77.7
4	82.6	52.5
5	42.3	57.4
6	51.1	48.7
7	46.0	36.6
8	38.7	52.9
9	52.2	44.0

equal to the fracture toughness of the host rock. Table 1 is a compilation of the mode-I stress intensity factors, calculated using equation 7 of Pollard & Holzhausen (1979), for the dike terminations in Fig. 12(a). Fracture mechanics theory requires that these values be equal to the fracture toughness of the host rocks. The average value of $\cong 53$ MPa · $m^{1/2}$ is one to two orders of magnitude higher than values obtained from tests on laboratory samples (Atkinson 1984), and *in situ* values estimated for granitic rocks of the Sierra Nevada batholith by Segall & Pollard (1983). However, it is only slightly lower than *in situ* values estimated for sedimentary rocks on the Colorado Plateau by Delaney & Pollard (1981).

Growth of dike segments

Figure 13 illustrates how the cross-sectional area of the tensile failure zones increases as the dike segments

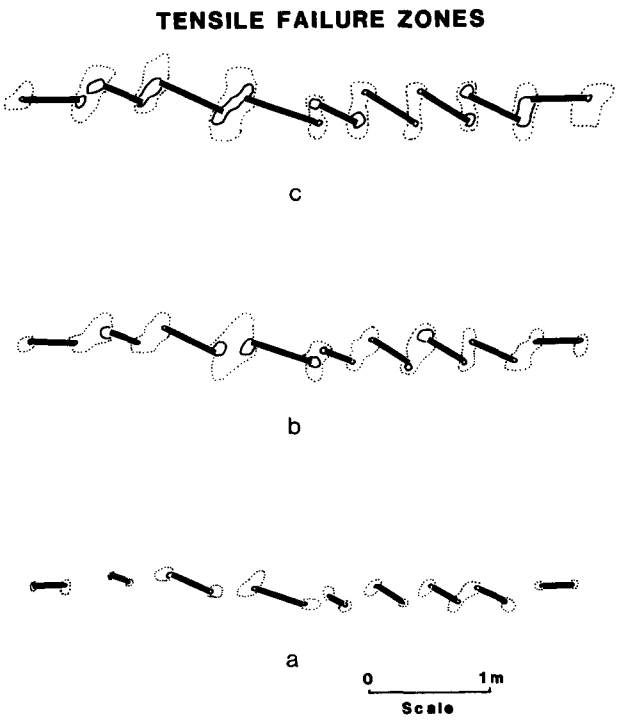

Fig. 13. Growth of the dike segments in Fig. 12. Thick solid bars represent the location and length of the dike segments for each calculation. The thin solid lines enclose areas where the least principal stress is tensile for dry host rocks and the thin dotted lines enclose areas where the least effective principal stress is tensile for interstitial fluids at 50 MPa. Dike segments lengthen progressively from (a) to (b) to (c) at 0.2 m increments.

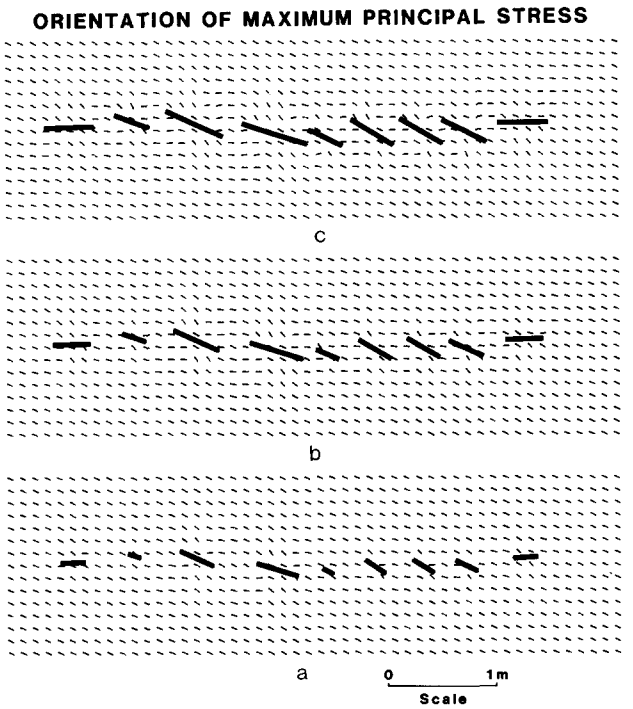

Fig. 14. Growth of the dike segments in Fig. 12. Thick solid bars represent the location and length of the dike segments for each calculation. The short dashes represent the orientation of the maximum compressive stress at selected locations around the dike segments. Dike segments lengthen progressively from (a) to (b) to (c) at 0.2 m increments.

lengthened during emplacement. For the initial calculation (Fig. 13a) each dike segment is 0.6 m shorter than in the final configuration (Fig. 12). At this stage of the dike emplacement the tensile failure zones are almost totally restricted to small zones at the end of each dike. As the propagation of the dike segments continues (Figs. 13b & c) the size of the tensile failure zones increases. The interaction between dike segments is revealed by the extension of the tensile failure zones between overlapping dike terminations, a feature that is especially evident for the calculations that assume an interstitial fluid is present in the host rocks (i.e. dotted lines on Fig. 13). It should be noted that fractures formed during the early stages of dike emplacement (Fig. 13a) are not accounted for in the calculations for the later stages.

Figure 14 gives the progressive distortion of the stress field during the emplacement of the dike segments in Fig. 9(a). The short lines on Fig. 14 show the orientation of the maximum principal stress at selected locations. During the early stages of dike emplacement (Fig. 14a) the distortion of the stress field is restricted to the areas between the dike segments and near the dike terminations. As dike emplacement proceeds (Figs. 14b & c) the geometry of the stress field changes with the largest distortion occurring in the area off the ends of the dike segments. In some cases the principal stress orientations can be rotated nearly 90° at distances of 0.25–0.5 m from the dike terminations (compare Figs. 14a & 12c).

Taken together, the results shown on Figs. 13 & 14 provide an explanation for dike-parallel fractures seen in Fig. 9(a). As the dikes were emplaced the tensile failure zones moved ahead of the dike terminus and enlarged during emplacement (Fig. 13). Initially, the maximum principal stress is oriented parallel to the dike segments in the area of tensile failure (Fig. 14a). As dike emplacement proceeds and the stress field becomes more distorted (Figs. 14b & c) the tensile failure zone includes areas where the orientation of the maximum principal stress is not parallel to the dike segments. However within the tensile failure zone there is always at least some area where the maximum principal stress is oriented parallel to the dike segments (Fig. 12). The points where the maximum principal stress orientations curve across the trends of the dike segments correspond well with the terminations of the chlorite veins and may have limited the propagation of these secondary fractures.

An additional factor to be considered in evaluating the distribution of chlorite veins is that the principal propagation direction was perpendicular to the plane of Fig. 9(a). Consequently, during the very earliest stage of dike emplacement a tensile failure zone probably developed along what is now the midsection of the dike segments.

DISCUSSION

Geometric and mineralogic features of mafic dikes and silica-rich chlorite veins within the Layered Series gabbros indicate that fractures hosting these dikes and veins were, for the most part, formed after the main stage hydrothermal activity associated with the cooling of the Skaergaard intrusion. The Layered Series gabbros deformed elastically during dike emplacement. It is likely that many of the fractures hosting the chlorite veins formed during dike emplacement and that these fractures represent fluid flow channels for localized hydrothermal systems associated with the cooling of the dikes. Reactions of fluids within these fracture systems produced the silica-rich chlorites and minor amounts of actinolite and quartz that now fill the fractures. The outcrops that we have studied have been affected by all of these processes. We have attempted to isolate data relevant to the study of one of these processes, fracturing associated with elastic deformation of the dike wall-rocks.

Laboratory studies of fracture propagation in rocks (Friedman *et al.* 1972, Hoagland *et al.* 1973, Swanson 1984) and ceramics (Wu *et al.* 1978, Rice *et al.* 1981) indicate that microfractures are created in the vicinity of the fracture tip. The area where these microfractures form has been called the "microfracture process zone". The tensile failure zone illustrated in Fig. 11 may be similar to the fracture process zone identified in laboratory studies though larger in scale. The microfractures developed in laboratory samples do not propagate as independent fractures, but the larger scale of the zone associated with the dikes may allow secondary fractures to develop and propagate in addition to the primary fracture that hosts the dike.

The anomalously high values of fracture toughness calculated above for the Layered Series gabbros may result from secondary fractures propagating during dike emplacement. Fracture mechanics theory relates fracture propagation to the energy required to create new fracture surfaces (Broek 1974, Lawn & Wilshaw 1975). Dike emplacement may require fracture energies high enough to propagate a population of fractures; the one hosting the dike plus any secondary fractures (Delaney *et al.* 1986).

The calculations summarized above (Fig. 11) suggest that the fracture process zone associated with the dikes cutting the Layered Series gabbros extended into the host rocks for distances of 1–5 m perpendicular to the trend of the dike. Field measurements indicate that fracture abundances as high as 10–15 m^{-1} occur marginal to dikes (Fig. 10 and Bird *et al.* 1987). These abundances commonly drop to 5 m^{-1} or less at distances greater than two meters from the dike margin. Consequently, in some cases as many as thirty or forty fractures may be propagating during dike emplacement. Our field observations suggest that it is more common for five to ten fractures to propagate as a group, but in some cases only one fracture, the one hosting the dike, propagated in isolation.

In the theoretical analysis presented above four important variables are critical to evaluating fracture propagation associated with dike emplacement. These variables are: magma pressure within the dike, magnitudes of the remote stresses, interstitial pore fluid pressure and elastic constants for the Layered Series gabbros. It is not possible to obtain absolute values for any of these variables and, in fact, the variables probably varied as a function of time and space during the deformation of the Skaergaard intrusion. Our analysis suggests that the difference between the remote principal stresses was between ≅25 and 50 MPa. Magma pressure within the dikes was probably approximately equal to the lithostatic load (125 MPa). Comparison of the elastic models presented above (Figs. 11–14) to distributions of fractures observed in the field suggests that interstitial fluids in the gabbroic host rocks were important for fracture initiation.

Acknowledgements—Field studies at the Skaergaard intrusion were conducted as part of the University of Arizona East Greenland expedition in 1982. This field work would not have been possible without the support and advice of D. L. Norton, C. K. Brooks, T. F. D. Nielsen, A. R. McBirney, M. T. Rosing and T. I. H. Anderson. Dave Pollard and an anonymous referee reviewed an earlier version of this manuscript and offered suggestions that greatly improved it. Various aspects of this study were supported by the National Science Foundation (NSF-EAR-8007828, NSF-EAR-8215120 and NSF-EAR-84-18129).

REFERENCES

Anderson, E. M. 1936. The dynamics of the formation of cone-sheets, ring-dykes and cauldron subsidences. *Proc. R. Soc. Edinb.* **56**, 128–157.

Atkinson, B. K. 1984. Subcritical crack growth in geological materials. *J. geophys. Res.* **89**, 4077–4114.

Beach, A. 1980. Numerical models of hydraulic fracturing and the interpretation of syntectonic veins. *J. Struct. Geol.* **2**, 425–438.

Birch, F. 1966. Compressibility, elastic constants. In: Handbook of Physical Constants (edited by Clark, S. P. Jr.). *Mem. geol. Soc. Am.* **97**, 97–174.

Bird, D. K., Rogers, R. D. & Manning, C. E. Mineralized fracture systems of the Skaergaard intrusion. *Meddelelser om Gronland.* In press.

Bird, D. K., Rosing, M. T., Manning, C. E. & Rose, N. M. 1985. Geological field studies of the Mikis Fjord area, East Greenland. *Bull. geol. Soc. Denmark* **34**, 219–236.

Brace, W. F. & Martin, R. J., III. 1968. A test of the law of effective stress for crystalline rocks of low porosity. *Int. J. Rock Mech. Min. Sci.* **5**, 415–426.

Bridgwater, D., Davies, F. B., Gill, R. C. O., Gorman, B. E., Myers, J. S., Pedersen, S. & Taylor, P. 1978. Precambrian and Tertiary geology between Kangerdluggsuaq and Anamagssalik, East Greenland. *Grönlands Geologiske Underogelse*, Rapport no. 83.

Broek, D. 1974. *Elementary Engineering Fracture Mechanics.* Noordhoff, Leyden.

Brooks, C. K. & Nielsen, T. F. D. 1982. The E. Greenland continental margin: a transition between oceanic and continental magmatism. *J. geol. Soc. Lond.* **139**, 265–275.

Brooks, C. K. & Platt, R. G. 1975. Kaersutite-bearing gabbroic inclusions and the late dike swarm of Kangerdlugssauq, East Greenland. *Mineralog. Mag.* **40**, 259–283.

Currie, K. L. & Ferguson, J. 1970. The mechanism of intrusion of lamprophyre dykes indicated by offsetting of dykes. *Tectonophysics* **9**, 525–535.

Deer, W. A., Howie, R. A. & Zussman, M. A. 1962. *Rock-Forming Minerals. Volume 3. Sheet Silicates.* Longman, Green & Co., London.

Delaney, P. T. 1982. Rapid intrusion of magma into wet rock: groundwater flow due to pore pressure increases. *J. geophys. Res.* **87**, 7739–7756.

Delaney, P. T. & Pollard, D. D. 1981. Deformation of host rocks and flow of magma during growth of the minette dikes and breccia-bearing intrusions near Ship Rock, New Mexico. *Prof. Paper U.S. geol. Survey* 1202.

Delaney, P. T., Pollard, D. D., Ziony, J. I. & McKee, E. H. 1986. Field relations between dikes and joints: emplacement processes and paleostress analysis. *J. geophys. Res.* **91**, 4920–4938.

Friedman, M., Handin, J. & Alani, J. 1972. Fracture surface energy of rocks. *Int. J. Rock Mech. Min. Sci. Geomech. Abstr.* **9**, 757–766.

Handin, J., Hager, R. V., Jr., Friedman, M. & Feather, J. N. 1963. Experimental deformation of sedimentary rocks under confining pressure: Pore pressure tests. *Bull. Am. Ass. Petrol. Geol.* **47**, 717–755.

Heard, H. C. & Page, L. 1982. Elastic moduli, thermal expansion and inferred permeability of two granites to 350° C and 55 megapascals. *J. geophys. Res.* **87**, 9340–9348.

Hoagland, R. G., Hahn, G. T. & Rosenfield, A. R. 1973. Influence of microstructure on fracture propagation in rock. *Rock Mech.* **5**, 77–106.

Kaitaro, S. 1952. On some offset structures in dilation dikes. *Bull. Comm. Geol. Finlande* **157**, 67–74.

Knapp, R. B. & Knight, J. E. 1977. Differential thermal expansion of pore fluids: fracture propagation and microearthquake production in hot pluton environments. *J. geophys. Res.* **82**, 2515–2522.

Knapp, R. B. & Norton, D. 1981. Preliminary numerical analysis of processes related to magma crystallization and stress evolution in cooling pluton environments. *Am. J. Sci.* **281**, 35–68.

Koide, H. & Bhattacharji, S. 1975. Formation of fractures around magmatic intrusions and their role in ore localization. *Econ. Geol.* **70**, 781–799.

Kokelaar, B. P. 1982. Fluidization of wet sediments during the emplacement and cooling of various igneous bodies. *J. geol. Soc. Lond.* **139**, 21–33.

Larsen, H. C. 1978. Offshore continuation of East Greenland dyke swarm and North Atlantic ocean formation. *Nature, Lond.* **274**, 220–223.

Lawn, B. R. & Wilshaw, T. R. 1975. *Fracture of Brittle Solids.* Cambridge University Press, Cambridge.

Manning, C. E. & Bird, D. K. 1986. Hydrothermal clinopyroxenes of the Skaergaard intrusion. *Contr. Min. Petrol.* **92**, 437–447.

Marsh, B. D. 1982. On the mechanics of igneous diapirism, stoping and zone melting. *Am. J. Sci.* **282**, 808–855.

McBirney, A. R. & Noyes, R. M. 1979. Crystallization and layering of the Skaergaard intrusion. *J. petrol.* **20**, 487–554.

Myers, J. S. 1980. Structure of the coastal dyke swarm and associated plutonic intrusions of East Greenland. *Earth Planet. Sci. Lett.* **46**, 407–418.

Nicholson, R. & Pollard, D. D. 1985. Dilation and linkage of echelon cracks. *J. Struct. Geol.* **7**, 583–590.

Nielsen, T. F. D. 1978. The Tertiary dike swarms of the Kangerdlugssuaq area, East Greenland: An example of magmatic development during continental break-up. *Contr. Min. Petrol.* **67**, 63–78.

Norton, D., Taylor, H. P., Jr. & Bird, D. K. 1984. The geometry and high-temperature deformation of the Skaergaard intrusion. *J. geophys. Res.* **89**, 10178–10192.

Page, L. & Heard, H. C. 1981. Elastic moduli, thermal expansion and inferred permeability of Climax quartz monzonite and Sudbury gabbro to 500°C and 55 MPa. *Proc. Symp. Rock Mech.* **22**, 97–104.

Paris, P. C. & Sih, G. C. 1965. Stress analysis of cracks. In: Fracture toughness testing. *ASTM STP* no. 381, Philadelphia, 30–83.

Pollard, D. D. 1973. Derivation and evaluation of a mechanical model for sheet intrusions. *Tectonophysics* **19**, 233–269.

Pollard, D. D. 1977. Fortran computer program for calculation of stress-intensity factors, stresses and displacements associated with a fluid-pressurized fracture near the earth's surface. *U.S. Geol. Surv*, open file report no. 78-160.

Pollard, D. D., Delaney, P. T., Duffield, W. A. & Endo, E. T. 1983. Surface deformation in volcanic rift zones. *Tectonophysics* **94**, 541–584.

Pollard, D. D. & Holzhausen, G. 1979. On the mechanical interaction between a fluid-filled fracture and the earth's surface. *Tectonophysics* **53**, 27–57.

Pollard, D. D. & Muller, O. H. 1976. The effect of gradients in regional stress and magma pressure on the form of sheet intrusions in cross section. *J. geophys. Res.* **81**, 975–984.

Pollard, D. D., Segall, P. & Delaney, P. T. 1982. Formation and interpretation of dilatant echelon cracks. *Bull. geol. Soc. Am.* **93**, 1291–1303.

Rice, R. W., Freiman, S. W. & Becher, P. F. 1981. Grain-size dependence of fracture energy in ceramics. I. Experiment. *J. Am. ceram. Soc.* **64**, 345–350.

Roberts, J. L. 1970. The intrusion of magma into brittle rocks. In: *Mechanism of Igneous Intrusion* (edited by Newall, G. & Rast, N.). Gallery Press, Liverpool, 287–338.

Robson, G. R. & Barr, K. G. 1964. The effect of stress on faulting and minor intrusions in the vicinity of a magma body. *Bull. Volcan.* **27**, 315–329.

Savage, J. C. & Cockerham, R. S. 1984. Earthquake swarm in Long Valley Caldera, California, January 1983: evidence for dike inflation. *J. geophys. Res.* **89**, 8315–8324.

Segall, P. & Pollard, D. D. 1980. Mechanics of discontinuous faults. *J. geophys. Res.* **85**, 4337–4350.

Segall, P. & Pollard, D. D. 1983. Joint formation in granitic rock of the Sierra Nevada. *Bull. geol. Soc. Am.* **94**, 563–575.

Simmons, G. & Brace, W. F. 1965. Comparison of static and dynamic measurements of compressibility of rocks. *J. geophys. Res.* **70**, 5649–5656.

Sneddon, I. N. & Lowengrub, M. 1969. *Crack Problems in the Classical Theory of Elasticity*. John Wiley, New York.

Soper, N. J., Higgins, A. C., Downie, C., Matthews, D. W. & Brown, P. E. 1976. Late Cretaceous-early Tertiary stratigraphy of the Kangerdlugssauq area, East Greenland and the age of opening of the north-east Atlantic. *J. geol. Soc. Lond.* **132**, 85–104.

Spence, D. A. & Turcotte, D. L. 1985. Magma-driven propagation of cracks. *J. geophys. Res.* **90**, 575–580.

Swanson, P. L. 1984. Subcritical crack growth and other time- and environment-dependent behavior in crustal rocks. *J. geophys. Res.* **89**, 4137–4152.

Vincent, E. A. 1953. Hornblende-lamprophyre dykes of basaltic parentage from the Skaergaard area, East Greenland. *J. geol. Soc. Lond.* **190**, 21–50.

Wager, L. R. & Brown, G. M. 1967. *Layered Igneous Rocks*. W. H. Freeman, San Francisco.

Wager, L. R. & Deer, W. A. 1938. A dyke swarm and crustal flexure in East Greenland. *Geol. Mag.* **75**, 39–46.

Wager, L. R. & Deer, W. A. 1939. Geologic investigations in East Greenland, Part III. The petrology of the Skaergaard intrusion, Kangerdlugssuaq, East Greenland. *Meddelelser om Grönland* **105**, no. 4.

Weertman, J. 1971. Theory of water-filled crevasses in glaciers applied to vertical magma transport beneath oceanic ridges. *J. geophys. Res.* **76**, 1171–1183.

Wu, C. C., Freiman, S. W., Rice, R. W. & Mecholsky, J. J. 1978. Microstructural aspects of crack propagation in ceramics. *J. Mater. Sci.* **13**, 2659–2670.

Wyss, M. 1970. Stress estimates for South American shallow and deep earthquakes. *J. geophys. Res.* **75**, 1529–1544.

Zoback, M. D. 1983. State of stress in the lithosphere. *Rev. Geophys. Space Phys.* **21**, 1503–1511.